How to Cite: Saidmuhamedova, M.Q., Turdiqulov, I.H., Atakhanov, A.A., Ashurov, N.Sh., Abdurazakov, M., Rashidova, S.Sh., & Surov, O.V. (2023) Biodegradable Polyethylene-Based Composites Filled with Cellulose Micro- and Nanoparticles. *Eurasian Journal of Chemistry, 110(2), 94-106.* https://doi.org/10.31489/2959-0663/2-23-16

Article

Received: 10 May 2023 | Revised: 24 May 2023 |
Accepted: 02 June 2023 | Published online: 06 June 2023

UDC 544.42+519.242.7

https://doi.org/10.31489/2959-0663/2-23-16

Mukhlisa Q. Saidmuhamedova[1], Islom H. Turdiqulov[1], Abdumutolib A. Atakhanov[1*], Nurbek Sh. Ashurov[1], Muhitdin Abdurazakov[1], Sayyora Sh. Rashidova[1], Oleg V. Surov[2]

[1] *Institute of Polymer Chemistry and Physics, Tashkent, Uzbekistan*
[2]*G.A. Krestov Institute of Solution Chemistry, Ivanovo, Russia*
*(*Corresponding author's e-mail: a-atakhanov@yandex.com)*

Biodegradable Polyethylene-Based Composites Filled with Cellulose Micro- and Nanoparticles

Composite materials filled with cellulose particles (microcrystalline cellulose and nanocellulose) have good prospects for use in various fields. Microcrystalline cellulose (MCC) and nanocellulose (NC) were isolated by chemical and physical methods and investigated. Composite materials based on polyethylene (PE) were obtained using MCC and NC as fillers (5–20 wt.%) and maleic anhydride grafted low molecular weight polyethylene (MA-g-LMPE) as a compatibilizer. The structure and morphology of the composites and fillers were characterized by Fourier transform infrared (FTIR) spectroscopy, X-ray diffraction, thermal analysis (TA), transmission electron microscopy (TEM), atomic force microscopy (AFM), and the strength properties were determined by tensile testing. An increase in the crystallinity index and mechanical strength of composites at low filler contents (up to 5 wt.%) was revealed. The size of the cellulose particles significantly affects the structure and properties of composites. Although the general picture of the effect of fillers on the crystalline structure and mechanical properties is similar, the addition of NC had a greater effect than MCC. The results of this study showed the possibility of using MCC and NC as reinforcement materials in composites, and they have biodegradable properties.

Keywords: cellulose microparticles, nanoparticles; polyethylene, composites, mechanical properties, biodegradability.

Introduction

Composite materials based on synthetic polymers reinforced with natural polymers, due to their unique physical, mechanical and operational characteristics, are widely used in various engineering fields [1–3]. Adding fillers based on natural polymers to synthetic polymers creates new materials with specific properties, including biodegradability after their end-of-life [4–6]. Micro- and nanoparticles of cellulose have good prospects in terms of their use as fillers for the preparation of composite materials due to their low density, large surface area, high mechanical properties, low toxicity, biodegradability, and renewability as raw materials [7–12]. Cellulose and its derivative-containing composites have been prepared and investigated for a wide range of vinyl polymers [13], including polycaprolactone, polyhydroxyalkanoate [14], polylactic acid [15], thermoplastic starch [16], polyacrylamide [17] and others.

The structure of polymer composites is determined not only by mixing conditions, but also by the dispersion of the polymer filler, which retains its particle shape during mixing, and the uniformity of its distribution in the polymer matrix. The effect of dispersed filler particles on the crystallization process of polyolefin was studied, and it was found that there are numerous crystallization centres on the filler surface, on which polymer crystallites grow; as a result, the crystallinity index increases [18, 19]. Filler particles are stiffer and harder than matrix materials, so they reinforce the polymer matrix. The filler addition into the polypropylene/polyethylene (PP/PE) polymer matrix increases the strength and stiffness, but reduces the elasticity of the materials [20, 21]. To eliminate the negative effect of the filler on the elasticity of polymer composites, functionalization of both polyolefin (insertion of hydrophilic groups) [22, 23] or fillers (insertion of hydrophobic groups) [24–26] has been suggested, and the addition of elastomers [27, 28] or compatibilizers [29, 30] could be used. Compatibilizers consisting of polar and nonpolar parts are located in the interfacial region, increasing the interaction between the nonpolar polymer and the polar filler and contributing to a uniform distribution of the filler.

The size and shape of the filler particles significantly affect the physical and mechanical properties of composites. Composites containing highly dispersed fillers are stronger and less viscous [31]. Moreover, oblong filler particles are stronger reinforcing agents for the polymer matrix than spherical particles [32].

The addition of functional groups into the structure of cellulose reduces its thermal stability. The process of partial esterification of cellulose occurs as cellulose nanoparticles are formed by acid hydrolysis with highly concentrated solutions of sulfuric acid [33]. At the same time, the presence of sulfate groups in the nanocellulose composition leads to lower temperature thermal stability [34, 35], which makes it difficult to use nanocellulose in high-temperature processes. Therefore, we used a hydrochloric acid solution to extract cellulose nanoparticles.

In the present work, polymer composites based on polyethylene filled with cellulose micro- and nanoparticles were obtained and their structure and properties were studied.

Experimental

Chemicals and Materials

The following chemicals and materials were used: sodium hydroxide (NaOH, 99 %), hydrogen peroxide (H_2O_2, 60 %), nitric acid (HNO_3, 65 %) and hydrochloric acid (HCl, 37 %) purchased from Fortek Ltd., Tashkent, Uzbekistan. Low-density polyethylene (PE, produced by JV "Shurtan Gas Chemical Complex" Comp. Limit., Uzbekistan) was used as a polymer matrix in compounds. Low-molecular-weight polyethylene (LMPE) with a number-average molecular weight (Mn) of 1000–2000 was supplied by JV "Uz-Kor Gas Chemical" Co. Ltd., Uzbekistan. Benzoyl peroxide (BP, 75 %), a free radical initiator, maleic anhydride (MA, 98 %), a monomer, styrene (99 %), a chain transfer agent, acetone (99.5 %), a wash solution for the products and xylene (90 %), a solvent for the initiator, were purchased from Sigma–Aldrich, USA.

Cotton Cellulose Extraction

Cotton cellulose (CC) was extracted by heating cotton linter in a 1 M sodium hydroxide solution at 120 °C for 2 h to remove hemicellulose and lignin, as reported previously [36]. It was washed with distilled water to a neutral pH solution and bleached at 120 °C for 2 h using 4 % hydrogen peroxide. The bleached fibres were filtered, and washed several times with distilled water, and dried at 100 °C for 4 h. CC had a degree of polymerization (DP) of 1200, and was used to prepare MCC.

MCC Extraction

MCC was extracted from CC by acid hydrolysis [36]. 50 g of CC was placed in a glass container and hydrolysed with 500 mL of a 4 % aqueous nitric acid solution at a boiling temperature of 100–105 °C for 2 h. The hot acid mixture was poured into 2.5 L of cold water, and the mixture was vigorously stirred with a spatula and allowed to stand overnight. The MCC obtained by this process was filtered, washed with distilled water until a neutral pH value, filtered, and dried at 100 °C for 4 h. The MCC was used to obtain nanoparticles of cellulose.

NC Isolation

NC was isolated using a reported protocol with modification [37]: the MCC (20 g) was hydrolysed with a hydrochloric acid solution (400 mL, 4N) at 70 °C for 60 min. The suspension was diluted 10-fold with cold water (5 °C), centrifuged, and dialysed until a neutral pH value, and the aqueous suspension was dispersed via ultrasonication for 1 h and homogenization for 1 h. Finally, the sample was freeze-dried.

Synthesis of compatibilizer (MA-g-LMPE)

The compatibilizer (MA-g-LMPE) was synthesized by reacting LMPE with MA according to a published method with slight modification [38]. The experiment was performed in a three-neck 250 mL round-bottom flask with a magnetic stirrer, a nitrogen inlet, and a thermometer. In a typical experiment, the reaction flask was heated in an oil bath to melt the LMPE. When the LMPE was melted completely, selected amounts of MAH and styrene were added to the flask. When the system reached homogeneity, the initiator was dissolved in xylene and added to the reaction flask. A small nitrogen flow passed through the flask during the whole reaction process. After the specified time, the reaction was stopped, and the grafted copolymer was precipitated in acetone. The precipitate was washed with acetone and filtered repeatedly to remove unreacted MAH, then dried in a vacuum oven at 60 °C to a constant weight. The compatibilizer was used as an agent to improve the compatibility of the PE and natural fillers (MCC, NC).

Composites Preparation

Compounding

Composites were prepared by high-temperature shear deformation on a rotary laboratory mixer (Brabender) at 190±2 °C. The mixture was ground for 20 min at 50 rpm. The ratios of natural fillers (MCC, NC)

to PE used in this study were (5÷95), (10÷90) and (20÷80) wt.%. The compatibilizer MA-g-LMPE was also added at 5 wt.% based on the weight of PE. Both PE and MA-g- LMPE were first melted at 170 °C, then the fillers (MCC, NC) were added.

Forming composite samples

The composites were placed in a hot compression moulding machine (Zamak, Poland) to form quadrangle-shaped composites to be used in mechanical testing. The composite samples were preheated in the mould at 180 °C for 3 min to ensure complete melting at atmospheric pressure. Then a pressure of 6 bars was applied to the mould and held for 5 min under constant temperature and pressure to form composites. After that, the forms were chilled and removed. In each tensile test, 1.5 g of sample was used to form a composite sheet with dimensions of 10 mm (width) × 75 mm (length) × 2 mm (thickness).

Characterization Methods

FTIR

The structure of samples was determined by the FTIR spectrometer "Inventio-S" (Bruker). FTIR spectra were recorded in the transmission mode in 400–4000 cm^{-1} wavenumber range with a resolution of 2 cm^{-1} and 32 scans at a temperature of 25 °C. The OPUS software was applied to determine the peaks at specific points. The samples were pressed in pellets under pressure 300 MPa containing 1 mg of the compound to be analyzed and 100 mg of potassium bromide.

Wide-angle X-ray diffraction

XRD studies were carried out according to a previously published method with a slight modification [39] on a XRD Miniflex 600 (Rigaku, Japan) with monochromatic CuKα radiation isolated by a nickel filter with a wavelength of 1.5418 Å at 40 kV and a current of 15 mA. The spectrum was recorded in the interval 2θ = 5°–40°. The data processing of experimental diffraction patterns, peak deconvolution, describing the peaks used by Miller indices, peak shape, and the basis for the amorphous contribution were conducted using the "SmartLab Studio II" software and PDF-2 (2020 Powder diffraction file, ICDD) data base.

The crystallite size, τ (Å), was calculated by the Scherrer equation [40, 41]:

$$\tau = \frac{K \cdot \lambda}{\beta \cdot \cos\theta},$$

where K — the correction factor (0.9); λ — the wavelength of the X-ray radiation (1.5418 Å); β — the full width at half maximum of the diffraction peak in radians; θ — the diffraction angle of the peak.

The crystal index (*CrI*) (%) was calculated by the following equation:

$$CrI = \frac{I_t - I_a}{I_t} \cdot 100,$$

where I_t — the total intensity; I_a — the amorphous intensity.

Thermal Analysis

Thermal analysis of the samples was recorded on a STA TG-DTA/DSC "Start-1600" (Linseis) by heating ~5 mg of samples at 10 °C/min in air atmosphere from ambient temperature to 700 °C. The results obtained by the TA method were used to calculate the crystallinity index of the polymer in composites [42], which was calculated based on the analysis of the DSC curves:

$$\chi_c = \frac{\Delta H_m}{w \Delta H_m^o},$$

where χ_c — the crystallinity index; ΔH_m — the enthalpy of the composite melting; w — the mass fraction of polymer in the composite; $\Delta H_m°$ — the enthalpy of the melting of neat polymer (χ=100 %).

TEM

Transmission electron microscopy studies were performed using PEM-100 equipment with a high accelerating voltage of 80 kV and a magnification of 104 times. The samples were prepared by the suspension method, and the studied samples were applied to a supporting film with carbon tinting after the sample was dried and contrasted with joint evaporation of platinum and carbon (in percentages of 85:15) at an angle of 45°.

AFM

Structural studies were also performed using an Agilent 5500 atomic force microscope (Agilent). Silicon cantilevers with a stiffness of 9.5 N/m^2 and a frequency of 145 kHz were used. The maximum AFM scanning area (x÷y÷z) is 25÷25÷1 μm. Calculations of particle size distribution by width and length were carried out using MountainsMap Premium Software, Version 6.2 (USA).

Optical Microscopy

The surface of the composites was observed by "BA 210 Digital" (Motic) optical microscope.

Sorption Measurements

The sorption measurements were carried out using a McBain balance with quartz spirals of 1 mg/mm sensitivity in the relative humidity (*P*/*Ps*) range 0.10–1.0 at 25 °C until sorption equilibrium was established. The change in sample mass during the sorption process was observed using a KM-8 cathetometer.

Mechanical properties of composites

Measurements of the mechanical properties (tensile strength (σ) and elongation (L)) of the composites were performed using an AG-X plus tensile tester (Shimadzu) according to standard methods at a 50 mm/min crosshead speed.

Statistical analysis

All experimental data were collected in triplicates and data expressed as average ± standard deviation. Data were compared using a one-way ANOVA with post-Bonferroni test using Graph-Pad Prism 5.04 (GraphPad Software Inc.)

Results and Discussion

FTIR studies (Fig. 1) showed that the spectra of NC and MCC are characteristic of cellulose; however, the intensities of the NC spectra were higher. Valence vibrations of the hydroxyl groups involved in intermolecular and intramolecular hydrogen bonds appeared at approximately 3400 cm^{-1}. Valence vibrations of the C-H bonds in the methylene groups of cellulose appeared in the region of 2895 cm^{-1}, vibrations of adsorbed water molecules appeared in the region of 1635 cm^{-1}. The absorption bands in the regions of 1420 cm^{-1}, 1335-1375 cm^{-1}, 1202 cm^{-1}, and 1075-1060 cm^{-1} corresponded to the strain vibrations of -H, -CH_2, -OH, and -CO and the valence vibrations of the C-O pyranose ring.

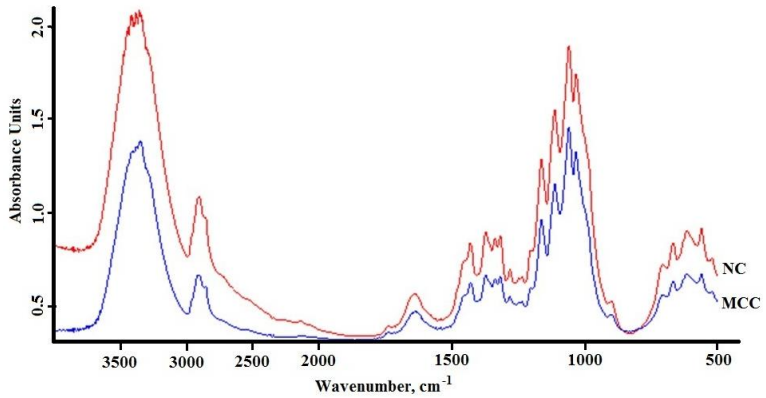

Figure 1. FTIR spectra of NC and MCC

The X-ray diffraction study showed that acid hydrolysis led to an increase in the crystallinity index of NC associated with the removal of the amorphous cellulose structure. Four crystal reflexes were observed at approximately 2θ=14.65°, 16.35°, 22,61° and 35.07° corresponding to the (10-1), (101), (002) and (040) planes (Fig. 2). The results of X-ray analysis show that during acid hydrolysis, the interplanar distance decreased, and the crystal reflexes shifted towards larger values. The unit cell size of NC was lower than that of MCC (Table 1).

Table 1

Structural parameters of NC and MCC

Options	MCC			NC		
	Crystalline Reflexes					
	10-1	101	002	10-1	101	002
Position of the maximum *2θ*, (deg.)	14.48	15.94	22.56	14.65	16.35	22.61
Interlunar spacing *d*, (Å)	6.11	5.55	3.94	6.04	5.42	3.93
Crystallite size *l*, (Å)	50.4	53.9	66.5	45.2	43.8	66.3
Crystallinity index, %	86			92		
Elementary cell size, a÷b÷c (Å)	8.65÷10.36÷7.91			8.34÷10.23÷7.90		

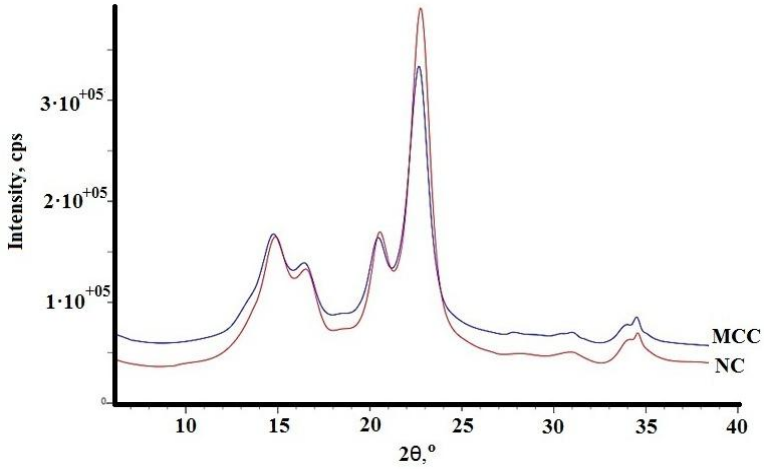

Figure 2. X-ray diffraction patterns of MCC and NC

TEM and AFM studies have shown that NC particles are in the form of whiskers with a particle size of 50–300 nm in length and 10–40 nm in width (Fig. 3 *a*, *b*). The particle size distribution ranged from 110 to 145 nm in length and 25–30 nm in width (Fig. 3 *c*, *d*).

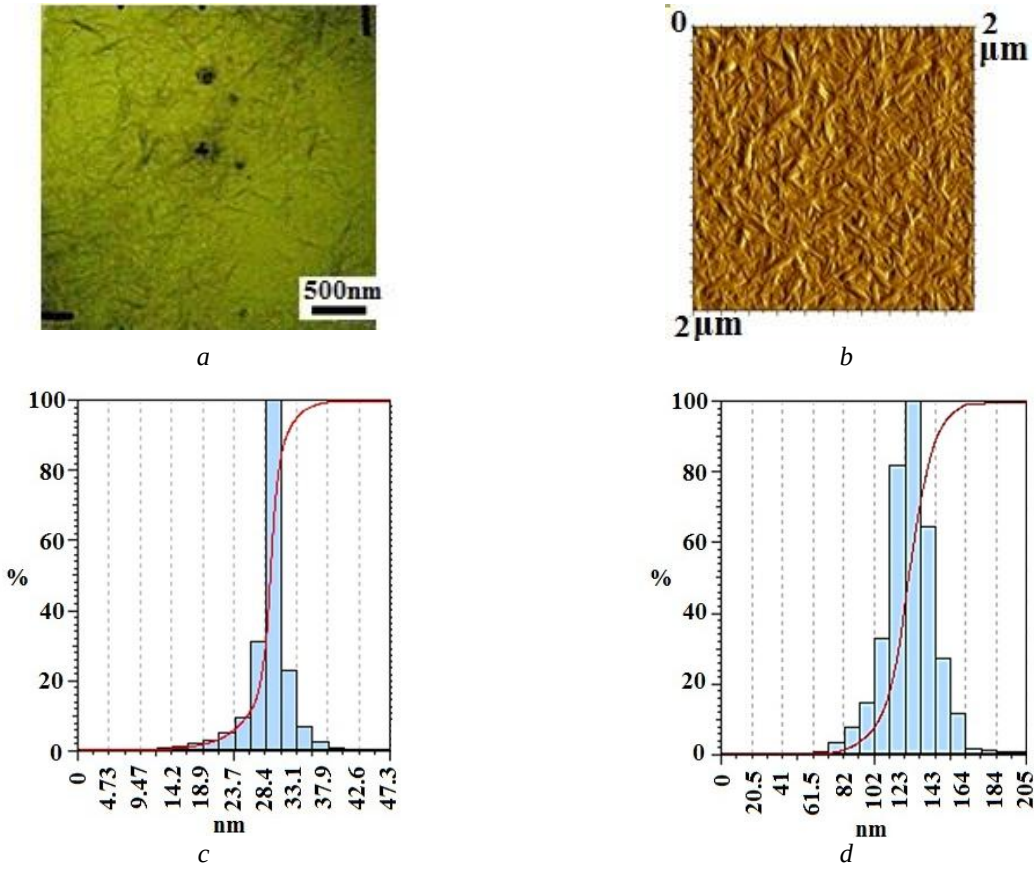

Figure 3. TEM (*a*) and AFM (*b*) images of NC and particle size distribution by width (*c*) and length (*d*)

Sorption studies using low molecular weight liquids (water and ethanol) were carried out for the NC and MCC, and the parameters of the capillary-porous structure of the samples were calculated based on isotherms of water vapour sorption (Fig. 4, Table 2).

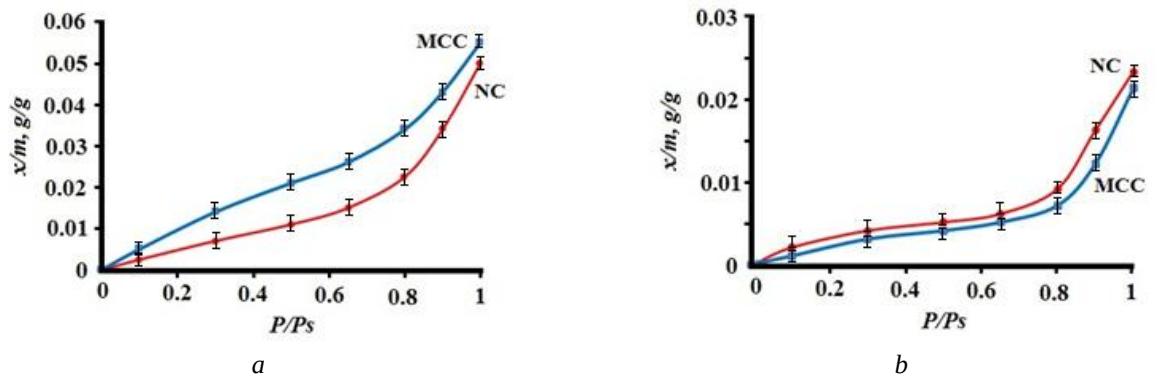

a *b*

Figure 4. Isotherms of water (*a*) and ethanol (*b*) vapour sorption by MCC and NC

It was found that X_m, S_{sp} and W_o of NC compared to MCC are lower in the case of water sorption and higher in the case of ethanol sorption. This is probably due to capillary condensation of water molecules on the polymer surface, since these parameters were calculated at 100 % relative humidity.

T a b l e 2

Parameters of the capillary-porous structure

Indicator	NC	MCC	NC	MCC
	Water sorption, %		Sorption of ethanol, %	
X_m, g/g	0.0052	0.0069	0.0034	0.0022
S_{sp}, m^2/g	18.28	24.44	12.21	7.38
W_o, cm^3/g	0.011	0.019	0.029	0.025
r_k, A_o	12.04	15.55	47.5	68.69
Note: Result presented as mean ±0.04 % standard deviation, n = 3.				

When filler is mixed with a synthetic polymer at the micro- and nanoscale, the components of the mixture form an interpenetrating mesh structure, which provides the filled polymer with the effect of additional degradation. It is known that filler can accumulate in the less ordered regions of the polymer structure. PE/filler composites at different ratios were investigated by FTIR and X-ray to establish the effect of the filler on the structure of PE.

FTIR spectra (Fig. 5) contain absorption bands at 2922 and 2850 cm^{-1} corresponding to the asymmetric and symmetric valence vibrations of CH_2 groups. The absorption bands of scissor and pendulum deformation vibrations of CH_2 groups occur at 1466 and 720 cm^{-1}. The absorption band corresponding to the region of approximately 750-700 cm^{-1} characterizes the crystalline phase of PE, while there is only one strong absorption band at 720 cm^{-1} in the amorphous phase [43, 44].

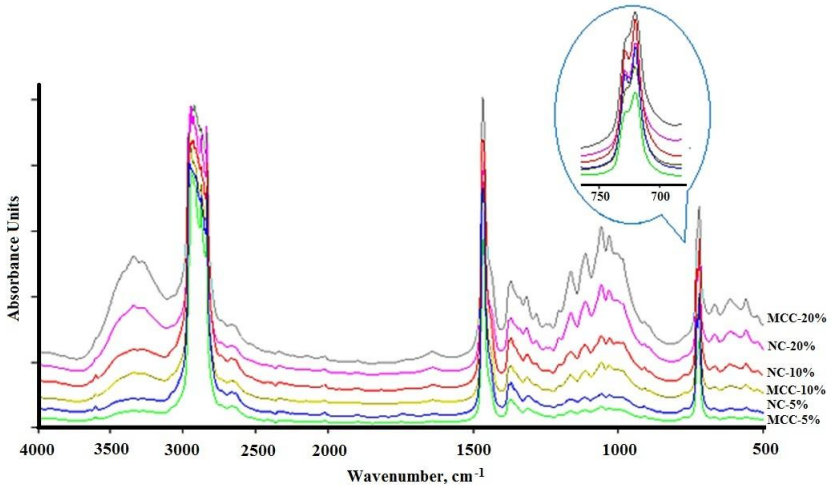

Figure 5. FTIR spectra of composites with different filler contents, wt.%: PE/MCC — 5, 10, 20 and PE/NC — 5, 10, 20

Characteristic cellulose bands are present in the 1017–1206 cm^{-1} range. The insertion of MCC and NC into PE leads to a shift of the 888 cm^{-1} band to the region of 853-861 cm^{-1}. It was also observed that some changes in the 1300–900 cm^{-1} region occur during heat treatment. This result seems to indicate the formation of PE with cellulose, inclusion compounds and H-complexes. The curves of the samples differ in the intensity of the characteristic bands at 1019, 1242, 1373, 1740 cm^{-1} and in the appearance of a new broad peak in the region of 3300-3500 cm^{-1}, which corresponds to the valence vibrations of OH-groups. More intense peaks were observed in the spectra of the PE/NC than in the spectra of the PE/MCC.

Two crystalline maximums of PE were observed in the X-ray diffraction patterns at 22° and 24.5°, corresponding to reflections (110) and (200) related to orthorhombic structure (Fig. 6). In addition, for all samples, one can observe a crystalline reflex relating to cellulose in the region of (200) corresponding to plane (110), and at high filler contents (20 %), weakly expressed reflexes relating to cellulose shifted at 15.5°, 17.2° corresponding to planes (101) and (10-1). Additionally, a decrease in the intensity of the PE crystal maximum at 24.5° and the appearance of a new crystal maximum related to cellulose in the region of 23.2° corresponding to the (10-2) plane were observed in the patterns of the same samples.

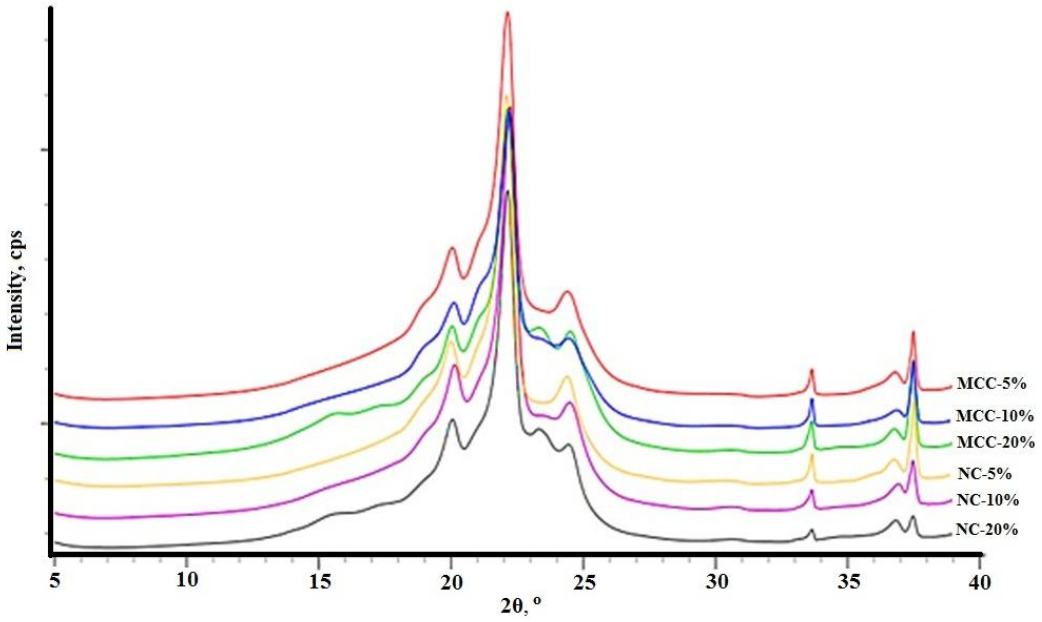

Figure 6. X-ray diffraction patterns of composites with different filler contents, wt.%:
PE/MCC — 5, 10, 20 and PE/NC — 5, 10, 20

The results showed that the crystallinity index values of all polymer composites differed from the χ of neat PE (Fig. 7).

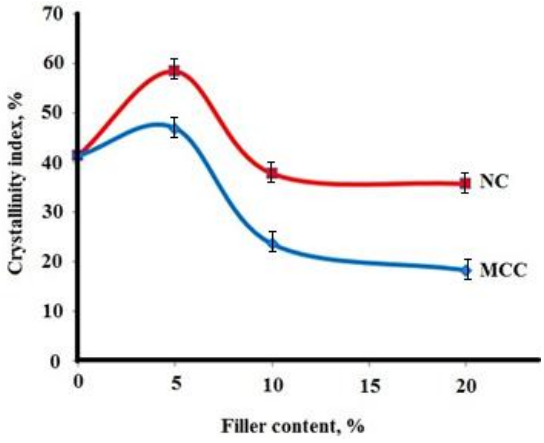

Figure. 7. Dependence of the crystallinity index of the composites on the filler content

The crystallinity was extremely dependent on the filler content and reached a maximum at a filler content of 5 wt.%. The presence of fillers up to this concentration led to the increase in the PE matrix values as an artificial seed for structure formation [45]. The reason for this behaviour may be the interphase phenomena that occur at the polymer-filler interface and the appearance of interfacial layers with characteristics that changed due to interfacial interactions.

An increase in the filler content in the range of 5–10 % led to a decrease in the crystallinity index. Most likely, an increased amount of filler contributed to their convergence; when they began to coagulate, the small particles aggregated into larger particles, while the specific surface area of the fillers decreased sharply, and, as a result, the active interactions of PE with the fillers decreased, and the fillers gradually began to have a lesser effect on the structure. A further increase in the amount of fillers up to 20 % somewhat suppressed the crystallization process and increased the number of defects in the crystallites and the amorphization of PE.

The dependence of the PE crystal lamella thickness on the filler content is shown in Figure 8. The thickness was calculated using Scherrer's formula by measuring the width at half the height of the high-intensity X-ray band corresponding to the reflections from the crystallographic planes (110).

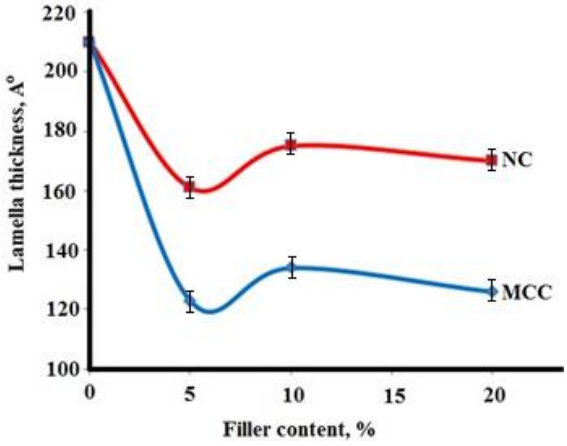

Figure 8. Dependence of lamella thickness on the filler content

As can be seen in Figure 8, the presence of fillers up to 5 % led to a decrease in the size of the crystallites because in these concentration intervals, there were many solid filler particles serving as artificial seed crystals for structure formation, as mentioned above. As a result, numerous crystallites formed, and their sizes were relatively smaller than that of neat PE. Despite a decrease in the thickness of the crystalline lamella at 5 % filler content, the PE crystallinity index reached its maximum value (Fig. 6) due to an increase in the total number of crystalline formations, the predominant number of which was crystallites grown on the artificial seed crystals. As a result, the crystallites, smaller dimensions of which enabled them to undergo denser packing in the amorphous structure, contributed to the increasing density of the final material. This reasoning is true if the growing crystalline formations filled the available amorphous space as much as possible when the growth of crystallites slowed upon meeting similar neighbouring formations.

A decrease in the χ values and the growth of the crystallites were observed in the range of filler content of 5–10 % (Fig. 7 and 8). A further increase in filler content up to 10–20 % partially suppressed the mobility of the PE macromolecules and the crystallization process, resulting in both a reduction in the crystallinity index and a decrease in crystallite size. The densities of fillers were different ($\rho_{NC} >> \rho_{MCC}$), and the denser filler particles had a more active effect on structure formation in the PE (Fig. 7).

Table 3

Crystallinity index (χ) and asymmetry index (AI) of PE and composites

PE/NC ratio, %	χ, %	AI	PE/MCC ratio, %	χ, %	AI
100:0	29	0,17	100:0	29	0,17
95:5	40	0,17	95:5	43	0,17
90:10	34	0,19	90:10	34	0,20
80:20	38	0,19	80:20	36	0,21

The thermal stability of a composite material is a desirable property in many applications. The thermal expansion of cellulose reinforced polyethylene composites has been studied using wood and fibrous cellulose as fillers [46, 47]. The viscose fibers and the MCC decreased the coefficients of the linear thermal expansion of the high density polyethylene (HDPE) matrix in the flow direction [48]. The effect of fillers on the crystalline structure of PE was also studied by thermal analysis. Calculations based on thermal analysis data showed that the values of the crystallinity index of all polymer composites were appreciably higher than the χ of neat PE (Table 3). The melting peak of the crystallizing polymer reflected the crystallite size distribution to some extent. The asymmetry of the melting peak was used to calculate indicators of the polymer crystal structure [49].

Similar results were obtained; the structure and properties of high density polyethylene-based composite films with different natural fillers (cellulose, soybean meal, and pellets) were studied [46]. Some increases in the crystallinity index and the proportion of perfect crystallites for HDPE with increasing filler content were noted. These increases occurred because the fillers acted as seed crystals in the crystal formation by forming films. We assumed that the reason for the increase in the crystallinity index was not only the presence of solid filler particles, but also the conditions of the polymer mixing process at a high temperature (180 °C). In this case, the dispersion component of the PE mixtures reflects the crystalline phase under the influence of the thermal field as it underwent modifying changes similar to those of the morphemes observed during the thermal treatment of the crystallizing polymers.

The crystallinity index values obtained by X-ray and thermal analyses do not coincide because these methods are based on the study of completely different physical and chemical phenomena. The crystallinity index of a polymer determined from X-ray data represents the total amount of ordered (crystalline) polymer areas that contribute to the coherent scattering of X-rays. When determining the crystallinity index by thermal analysis, the proportion of polymer macromolecules that are capable of absorbing energy during thermal influence and moving from an ordered to a disordered (molten) state is taken into account. However, it was noted that the general picture of the effect of fillers on the crystal structure of polyethylene remained consistent.

Optical studies have shown that filler particles can be observed in microphotographs and that their size depends on the filler. NC particles are small and needle-shaped, while MCC particles are larger.

Mechanical studies of the composites showed that filler content up to 5 % increased the strength of the composites (Fig. 9). This result is consistent with the X-ray results. Small additions of fillers that serve as structure formers contributed to the refinement of the spherulitic structure, changing the packing density of the structural elements of the spherules and the ordering of the structure of the crystallizing polymer. Apparently, these factors can increase the strength of the crystallizing polymer when small content filler is dispersed throughout the polymer matrix.

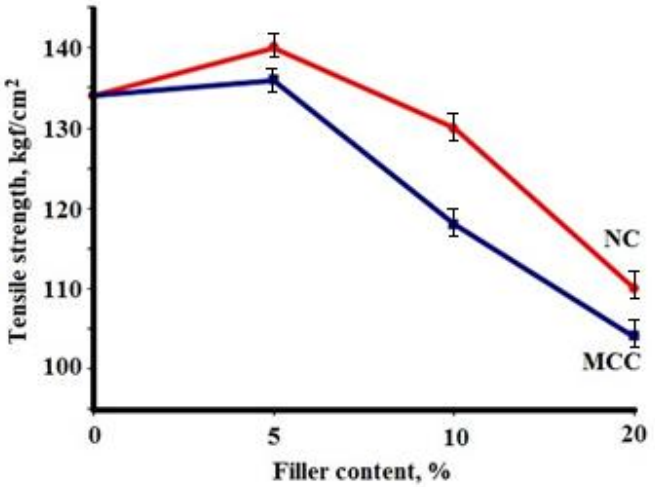

Figure 9. Mechanical characteristics of PE/MCC and PE/NC composites

As the filler content increased, a significant amount of filler particles accumulated in the polymer matrix, which no longer contributed to structure formation, and the amorphous regions stiffened. This behaviour

led to a sharp decrease in the deformation strength of the polymers with high filler contents and to brittle fracture [50].

The ability of composite materials based on polyolefin and natural fillers to be degraded and assimilated by microorganisms depends on a number of characteristics of the polymer matrix and filler, as well as the structure of the whole material. Polymer composite materials are released into the environment and exposed to physical, chemical, and biological factors [51, 52]. The properties of polymers, including their strength, colour, and shape, are irreversibly changed by degradation or ageing. The final stage of ageing is the mechanical destruction of the materials (fragmentation). Microorganisms play the main role in biological degradation. The biological degradation of composites by microorganisms includes several stages [53, 54]. The first stage of biodegradation of a synthetic polymer begins with adsorption of microorganisms on its surface; the surface hydrophility must increase for the penetration of a microorganism into the polymer structure. To test the surface hydrophility, the samples were placed in different media: water and sodium chloride solution.

A nonmonotonic change in mass was observed for all samples because the fractions with low molecular weights were washed out from the surface layers on the first day, and then the process stabilized. Some samples behaved differently based on their compositions, exhibiting sharp washout of surface layers in the first several days, followed by swelling and penetration of the solvent into the intermolecular space. The degree of polymer weight reduction depends on the percentage of soluble components, the particle size of the filler and the availability of the filler in the polymer matrix.

The change in the mechanical properties of the samples over time after composting in special humus was studied (Table 4).

Table 4

Physical-mechanical properties (tensile strain and elongation) of composites before and after burial in soil for 90 days

Sample	Filler content, %	Before burial in soil		After burial in soil for 90 days	
		Tensile strange, kgf/cm^2	Elongation, %	Tensile strange, kgf/cm^2	Elongation, %
PE/NC	5	140	175	122	125
	10	130	135	113	105
	20	110	100	99	85
PE/MCC	5	136	110	121	92
	10	118	60	109	52
	20	104	45	91	38
Note: Result presented as mean ±0.3 % standard deviation, n = 5					

As can be seen in Table 4, the mechanical strength of composites aged in the soil decreased after a certain time, and the greater the filler content was, the lower the strength. A decrease in the strength characteristics of composites enabled us to assume partial destruction of the structures of the composites; such degradation was probably connected with the initial stages of biodegradation of natural fillers in composites. The studies of the physical and mechanical properties of the composites clearly demonstrate qualitative changes in the structure of the composites during biodegradation. Changes occurring in the materials under the influence of degradation in the soil include changes in colour, loss of mass, biological fouling of the composites, and mechanical destruction.

Conclusions

A comparative study on the structures of MCC and NC was carried out, and the changes in structural characteristics were shown upon transition from microparticles to nanoparticles. Composites based on polyethylene filled with different contents of cellulose micro- and nanoparticles were obtained. The structure of the composition was studied by infrared spectroscopy, X-ray structure and thermal analyses, and the change in structure depended on the type and amount of the filler. The role of small (up to 5 wt.%) contents of polysaccharides on the structure formation of polyethylene has been revealed. It was shown that an increase in the presence of natural additives (up to 20 wt.%) leads to a decrease in the degree of polyethylene ordering, which also affects the mechanical properties of the composite. Preliminary data showed the propensity of the obtained compositions to biodegrade.

Acknowledgments

The authors acknowledge the Ministry of Higher Education, Science, and Innovation of the Republic of Uzbekistan for supporting this investigation.

References

1 Rogovina, S.Z., Prut, E.V., & Berlin, A.A. (2019). Composite materials based on synthetic polymers reinforced with natural fibers. *J. Polym. Sci. Part A Polym. Chem.*, *61*(4), 417–438. https://doi.org/10.1134/S0965545X19040084

2 Azman, M.A., Asyraf, M.R.M., Khalina, A., Petru, M., Ruzaidi, C.M., Sapuan, S.M., Wan, N.W.B., Ishak, M.R., Ilyas, R.A., & Suriani, M.J. (2021). Natural fibre reinforced composite material for product design: a short review. *Polymers*, *13*(12), 1917. https://doi.org/10.3390/polym13121917

3 Nurazzi, N., Asyraf, M., Khalina, A., Abdullah, N., Aisyah, H., Rafiqah, S., Sabaruddin, F., Kamarudin, S., Norrrahim, M., Ilyas, R., & Sapuan, S. (2021). A review on natural fibre reinforced polymer composite for bullet proof and ballistic applications. *Polymers*, *13*(4), 646. https://doi.org/10.3390/polym13040646

4 Ibrahim, H., Farag, M., Megahed, H., & Mehanny, S. (2014). Characteristics of starch-based biodegradable composites reinforced with date palm and flax fibers. *Carbohyd. Polym.*, *101*, 11-19. https://doi.org/10.1016/j.carbpol.2013.08.051

5 Lu, D.R., Xiao, C.M., & Xu, S.J. (2009). Starch-based completely biodegradable polymer materials. *eXPRESS Polym. Let.*, *3*, 366–375. https://doi.org/10.3144/expresspolymlett.2009.46

6 Turdikulov, I.H., Mamadiyorov, B.N., Saidmuhammedova, M.Q., & Atakhanov, A.A. (2020). Obtaining and studying properties of biodestructable composite films based on polyethylene. *Open J. Chem.*, *6*(1), 030-036. https://doi.org/10.17352/ojc.000021

7 Omran, A.A.B., Mohammed, A.A.B.A., Sapuan, S.M., Ilyas, R.A., Asyraf, M.R.M., Koloor, S.S.R., & Petr, M. (2021). Micro- and nanocellulose in polymer composite materials: A review. *Polymers*, *13*, 231. https://doi.org/10.3390/polym13020231

8 Hao, W., Wanga, M., Zhou, F., Luo, H., Xie, X., Luo, F., & Cha, R. (2020) A review on nanocellulose as a lightweight filler of polyolefin composites. *Carbohyd. Polym.*, *243*, 116466. https://doi.org/10.1016/j.carbpol.2020.116466

9 Lee, K.Y., Aitomäki, Y., Berglund, L., Oksman, K., & Bismarck, A. (2014). On the use of nanocellulose as reinforcement in polymer matrix composites. *Combust. Sci. Technol.*, *105*, 15-27. https://doi.org/10.1016/j.compscitech.2014.08.032

10 Atakhanov, A.A., Kholmuminov, A.A., Mamadierov, B.N., Turdikulov, I.H., & Ashurov, N.Sh. (2020) Rheological Behavior of Nanocellulose Aqueous Suspensions. *J Polym Sci Part A Polym Chem.*, *62*(3), 213–217. https://doi.org/10.1134/S0965545X20030013

11 Shen, R., Xue, Sh., Xu, Y., Liu, Q., Feng, Z., Ren, H., Zhai, H., & Kong, F. (2020). Research progress and development demand of nanocellulose reinforced polymer composites. *Polymers*, *12*, 2113. https://doi.org/10.3390/polym12092113

12 Low, D.Y.S., Supramaniam, J., Soottitantawat, A., Charinpanitkul, T., Tanthapanichakoon, W., Tan, K.W., & Tang, S.Y. (2021) Recent developments in nanocellulose-reinforced rubber matrix composites: a review. *Polymers*, *13*, 550. https://doi.org/10.3390/polym13040550

13 Voronova, M.I., Surov, O.V., Kuziyeva, M.K., & Atakhanov, A.A. (2022). Thermal and mechanical properties of polymer composites reinforced by sulfuric acid-hydrolyzed and tempo-oxidized nanocellulose: a comparative study. *Chem. Chem. Tech.*, *65*(10), 95–105. https://doi.org/10.6060/ivkkt.20226510.6596

14 Valentini, F., Dorigato, A., Rigotti, D., & Pegotti, A. (2019). Polyhydroxyalkanoates/fibrillated nanocellulose composites for additive manufacturing. *J. Polym. Environ.*, *27*, 1333–1341. https://doi.org/10.1007/s10924-019-01429-8

15 de Souza, A.G., Barbosa, R.F.S., & Rosa, D.S. (2020) Nanocellulose from industrial and agricultural waste for further use in pla composites. *J. Polym. Environ.*, *28*, 1851–1868. https://doi.org/10.1007/s10924-020-01731-w

16 Csiszár, E., Kun, D., & Fekete, E. (2021) The role of structure and interactions in thermoplastic starch–nanocellulose composites. *Polymers*, *13*, 3186. https://doi.org/10.3390/polym13183186

17 Voronova, M.I., Surov, O.V., Afineevskii, A.V., & Zakharov, A.G. (2020). Properties of polyacrylamide composites reinforced by cellulose nanocrystals. *Heliyon*, *6*(11), e05529. https://doi.org/10.1016/j.heliyon.2020.e05529

18 Borysiak, S. (2013). Influence of cellulose polymorphs on the polypropylene crystallization. *J. Therm. Anal. Calorim.*, *113*, 281-289. https://doi.org/10.1007/s10973-013-3109-0

19 Robaidi, A.A., Anagreha, N., Addousb, M., & Massadeha, S. (2013). Crystallization behavior of iPP/LLDPE blend filled with nano kaolin particles. *Jordan J. Mech. Indust. Eng.*, *7*(1), 35-39.

20 Sanadi, A.R., Calufield, D.F., & Rowell, R.M. (1994). Reinforcing polypropylene with natural fibers. *Plast. Eng.*, *50*(4), 27-28.

21 Bledzki, A.K., & Jaszkiewicz, A. (2010). Mechanical performance of biocomposites based on PLA and PHBV reinforced with natural fibres. A comparative study to PP. *Compos. Sci. Tech.*, *70*(12), 1687-1696. https://10.1016/j.compscitech.2010.06.005

22 Peng, Y.C., Gallegos, S.A., Gardner, D.J., Han, Y., & Cai, Z.Y. (2016). Maleic anhydride polypropylene modified cellulose nanofibril polypropylene nanocomposites with enhanced impact strength. *Polym. Compos.*, *37*(3), 782-793. https://doi.org/10.1002/pc.23235

23 Hirai, S., Phanthong, P., Okubo, H., & Yao, S. (2020). Enhancement of the surface properties on polypropylene film using side-chain crystalline block copolymers. *Polymers*, *12*(11), 2736. https://doi.org/10.3390/polym12112736.

24 Nagalakshmaiah, M., Pignon, F., El Kissi, N., & Dufresne, A. (2016). Surface adsorption of triblock copolymer (PEO–PPO–PEO) on cellulose nanocrystals and their melt extrusion with polyethylene. *RSC Advances, 6*(70), 66224-66232. https://doi.org/10.1039/C6RA11139D

25 Zhang, Y.J., Jiang, X.Y., Bai, Z.W., Wang, J.K., Qian, Z.M., & Liu, Y.X. (2018). Re-treated nanocellulose whiskers alongside a polyolefin elastomer to toughen and improve polypropylene composites. *J. Appl. Polym., Sci. 135*(15), 46066. https://doi.org/10.1002/app.46066

26 Noguchi, T., Niihara, K., Iwamoto, R., Matsuda, G., Endo, M., & Isogai, A. (2021). Nanocellulose/polyethylene nanocomposite sheets prepared from an oven-dried nanocellulose by elastic kneading. *Compos. Sci. Technol., 207,* 108734. https://doi.org/10.1016/j.compscitech.2021.108734

27 Clemons, C. (2010). Elastomer modified polypropylene–polyethylene blends as matrices for wood flour–plastic composites. *Compos Part A, 41*(11), 1559–1569. https://doi.org/10.1016/j.compositesa.2010.07.002

28 Van de Velde, K., & Kiekens, P. (2001). Influence of fiber surface characteristics on the flax/polypropylene interface. *J. Thermopl. Compos. Mat., 14*(3), 244–260. https://doi.org/10.1106/13PW-MYJU-8HCJ-B1T1

29 He, X., Zheng, S., Huang, G., & Rong, Y. (2013). Solution grafting of maleic anhydride on low-density polyethylene: effect on crystallization behaviour. *J. Macromol. Sci. Phys., 52,* 1265–1282. https://doi.org/10.1080/00222348.2013.764217

30 Chang, M.K. (2015). Mechanical properties and thermal stability of low-density polyethylene grafted maleic anhydride/montmorillonite nanocomposites. *J. Ind. Eng. Chem., 27,* 96–101. https://doi.org/10.1016/j.jiec.2014.11.048

31 Fu, S-Y., Feng, X-Q., Lauke, B., & Mai Y-W. (2008). Effects of particle size, particle/matrix interface adhesion and particle loading on mechanical properties of particulate–polymer composites. *Compos. Part B Eng., 39*(6), 933-961. https://doi.org/10.1016/j.compositesb.2008.01.002

32 Essabir, H., Hilali, E., & Elgharad, A. (2013). Mechanical and thermal properties of bio-composites based on polypropylene reinforced with nut shells of Argan particles. *Mater. Design., 49,* 442-448. https://doi.org/10.1016/j.matdes.2013.01.025

33 Yuldoshev, Sh.A., Atakhanov, A.A., Sarimsakov, A.A. (2016). Cotton cellulose microcrystalline cellulose and nanocellulose: carboxymethyllation and oxidation reaction activity. *Nano Sci. Nano Tech., 10*(3), 102-109.

34 Voronova, M.I., Lebedeva, T.N., Surov, O.V., & Zakharov, A.G. (2013). Film properties of nanocrystalline cellulose with various contents of sulfate groups. *Khimiia Rastitelnogo Syria – Chemistry of plant materials, 3,* 49-57. https://doi.org/10.14258/jcprm.1303049

35 Zaini, L.H., Janoobi, M., Tahir, P.Md., & Karimi, S. (2013). Isolation and characterization of cellulose whiskers from kenaf bast fibers. *J. Biomater. Nanotech., 4,* 37-44. https://doi.org/10.4236/jbnb.2013.41006

36 Atakhanov, A.A., Mamadiyorov, B., Kuzieva, M., Yugay, S.M., Shahobutdinav, S., Ashurov, N.S., Abdurazakov, M. (2019). Comparative studies of physic-chemical properties and structure of cotton cellulose and its modified forms. *Khimiia Rastitelnogo Syria – Chemistry of plant materials, 3,* 5–13. https://doi.org/10.14258/jcprm.2019034554

37 Atakhanov, A., Turdikulov, I., Mamadiyorov, B., Abdullaeva, N., Nurgaliev, I., & Rashidova, S. (2019). Isolation of nanocellulose from cotton cellulose and computer modeling of its structure. *Open J. Polymer Chem., 9,* 117-129. https://doi.org/10.4236/ojpchem.2019.94010

38 Atakhanov, A.A., Turdikulov, I.K., & Ashurov, N.S. (2022). Polyethylene-based oxo-degradable nanocomposite film. *Rus. J. Appl. Chem., 95*(8), 1161–1168. https://doi.org/10.1134/S1070427222080110

39 Kuzieva, M., Atakhanov, A.,·Shakhobutdinov, S., Ashurov, N., Yunusov, Kh., & Guohua, J. (2023). Preparation of oxidized nanocellulose by using potassium dichromate. *Cellulose.* https://doi.org/10.1007/s10570-023-05222-8

40 Langford, J.I., & Wilson, A.J.C. (1978). Scherrer after sixty years: A survey and some new results in the determination of crystallite size. *J App Crystall 11*(2), 102-113.

41 Nam, S., French, A.D., Condon, B.D., & Concha, M. (2016) Segal crystallinity index revisited by the simulation of X-ray diffraction patterns of cotton cellulose I and cellulose II. *Carbohydr. Polym., 13,* 1-9. http://doi.org/doi:10.1016/j.carbpol.2015.08.035

42 Wendlandt, W.W. (1974). Thermal methods of analysis. A Willey-Interscience Publication John Wiley&Sons, New York.

43 Gorokhovatsky, Yu.A., Viktorovich, A.S., Temnov, D.E., Tazenkov, B.A., Aniskina, L.B., & Chistyakova, O.V. (2006). IK-spektroskopiia elektretov na osnove polietilena i polipropilena [IR spectroscopy of electrets based on polyethylene and polypropylene]. *Izvestiia Rossiiskogo Gosudarstvennogo Pedagogicheskogo Universiteta — Izvestia of the Russian State Pedagogical University named after A.I. Herzen, 6*(15), 69-75 [in Russian].

44 Ashurov, N.S., Shahobutdinov, S.S., Kareva, N.D., Yugay, S.M., Atakhanov, A.A., & Rashidova, S.S. (2020). Issledovanie struktury i svoistv nanostrukturnykh polimernykh smesei na osnove polietilena i polipropilena [Investigation of structure and properties of nanostructured polymer mixtures based on polyethylene and polyvinyl chloride]. *Plasticheskie massy – Plastics, 3-4,* 8-11. https://doi.org/10.35164/0554-2901-2020-3-4-8-11

45 Solomko, V.P. (1980). Napolnennye Kristallizuiushchiesia Polimery [Filled crystallizable polymers]. Nauk. Dumka, Kiev [in Russian].

46 Zhong, Y., Poloso, T., Hetzer, M., & De Kee, D. (2007). Enhancement of wood/polyethylene composites via compatibilization and incorporation of Organoclay particles. *Polym. Eng. Sci., 47*(6), 797–803. http://dx.doi.org/10.1002/pen.20756

47 Zhang, F., Qiu, W., Yang, L., Endo, T., & Hirotsu, T. (2002). Mechanochemical preparation and properties of a cellulose polyethylene composite. *J. Mater. Chem., 12,* 24–6. https://doi.org/10.1039/B108255H

48 Pöllänen, M., Suvanto, M., & Pakkanen, T.T. (2013). Cellulose reinforced high density polyethylene composites — Morphology, mechanical and thermal expansion properties. *Compo. Sci. Technol., 76,* 21-28. http://dx.doi.org/10.1016/j.compscitech.2012.12.013

49 Khvatov, A.V., Popov, A.A., Kolesnikova, N.N., & Lukanina, J.K. (2007). Biodegradable polymer composite materials. *J. Balkan. Tribological. Assoc., 13*(4), 527-535.

50 Normurodov, N.F., Berdinazarov, Q.N., Abdurazakov, M., Ashurov, N.R. (2022) Mechanical and Thermal Properties of Biodegradable Composites Based on graft copolymer LLDPE-g-MA/Gelatin. *Bulletin of the University of Karaganda Chemistry*, 108(4), 35-45. https://doi.org/10.31489/2022Ch4/4-22-11

51 Clemons, C. (2010). Elastomer modified polypropylene–polyethylene blends as matrices for wood flour–plastic composites. *Compos. Part A, 41*(11), 1559–1569. https://doi.org/10.1016/j.compositesa.2010.07.002

52 Albertsson, A.C., Andersson, S.O., & Karlsson, S. (1987). The mechanism of biodegradation of polyethylene. *Polym. Degrad. Stabil., 18,* 73-87. https://doi.org/10.1016/0141-3910(87)90084-X

53 Kawai, F. (1995). Break down of plastics and polymers by microorganisms. *Biochem. Eng., 52,* 151–194. https://doi.org/10.1007/BFb0102319

54 Matsumura, S. (2005). In: Smith R (ed) Mechanism of biodegradation, Wood head, London.

Information about authors*

Saidmuhamedova, Mukhlisa Qodir qizi — Junior researcher, Institute of Polymer Chemistry and Physics, 100128, Tashkent, Uzbekistan; e-mail: polymer@academy.uz; https://orcid.org/0000-0001-5592-4997;

Turdiqulov, Islom Hayitboy o'g'li — PhD, Junior researcher, Institute of Polymer Chemistry and Physics, 100128, Tashkent, Uzbekistan; e-mail: i.turdikulov@mail.ru; https://orcid.org/0000-0001-5100-7729;

Atakhanov, Abdumutolib Abdupatto o'g'li (corresponding author) — Doctor of technical sciences, Professor, Head of laboratory "Physic and physic-chemical methods of investigation" Institute of Polymer Chemistry and Physics, 100128, Tashkent, Uzbekistan; e-mail: a-atakhanov@yandex.com; https://orcid.org/0000-0002-4975-3658;

Ashurov, Nurbek Shodievich — Candidate of physic-mathematic sciences, Senior researcher, Institute of Polymer Chemistry and Physics, 100128, Tashkent, Uzbekistan; e-mail: ansss72@mail.ru; https://orcid.org/0000-0001-5246-434X;

Abdurazakov, Muhitdin — Candidate of technical sciences, Senior researcher, Institute of Polymer Chemistry and Physics, 100128, Tashkent, Uzbekistan; e-mail: muhitdin49@mail.ru; https://orcid.org/0000-0002-7950-6092;

Rashidova, Sayyora Sharafovna — Doctor of Science, Professor, Academician, Director of Institute of Polymer Chemistry and Physics, 100128, Tashkent, Uzbekistan; e-mail: polymer@academy.uz; https://orcid.org/0000-0003-1667-4619

Surov, Oleg Valentinovich — Doctor of Science, Professor, Senior researcher, G.A. Krestov Institute of Solution Chemistry, Ivanovo, Russia; e-mail: ovs@isc-ras.ru; https://orcid.org/0000-0002-7164-364X

*The author's name is presented in the order: *Last Name, First and Middle Names*